

Theoretical and experimental investigation of Z-pinch plasma as the source of a powerful pulse of soft x rays for the generation of shock waves in condensed targets

E. V. Grabovskii, V. P. Smirnov, and S. V. Zakharov

Troitsk Institute for Innovative and Thermonuclear Investigations, 142092 Troitsk, Moscow Province, Russia.

O. Yu. Vorob'ev, K. S. Dyabilin, M. E. Lebedev, V. E. Fortov, and A. A. Frolov

Research Center for the Thermophysics of Pulsed Effects, 127412 Moscow, Russia

(Submitted 22 June 1995)

Zh. Éksp. Teor. Fiz. **109**, 827–838 (March 1996)

The results are given of a theoretical analysis of the processes in a Z-pinch plasma in regimes that give rise to a powerful pulse of soft x rays. Attention is devoted to schemes with a double liner. Estimates of the radiation power and spectrum are discussed. The results are used to model processes that take place in the generation of a shock wave when soft x rays interact with a target. Experiments have been conducted on the generation of shock waves with pressures up to 3 Mbar in lead under the influence of soft x rays using the ANGARA-5 device. The results of the experiments are compared with the data of numerical modeling.

© 1996 American Institute of Physics. [S1063-7761(96)00903-1]

1. INTRODUCTION

The main problem in the use of concentrated fluxes of charged particles and laser radiation in controlled thermonuclear fusion¹ and in the dynamical physics of high energy densities² is associated with the strong spatial inhomogeneity of the power that is released. This leads to loss of symmetry of the spherical compression of the thermonuclear fuel and makes it difficult to generate plane shock waves in experiments to study matter under extreme conditions. One of the most effective ways of solving this problem is to use plasma x rays with a nearly thermal spectrum produced by the action on a target of fluxes of directed energy³ or by the electrodynamic compression of cylindrical shells in Z-pinch geometry.⁴ The almost plane shock waves excited by such radiation are an extremely simple form of self-similar hydrodynamic flow and may well be the most natural and effective source of experimental information both on the intensity of the incident x rays and on the physics of their interaction with condensed targets.

If a Z-pinch plasma is used as radiation source, the so-called double liner^{5–7} scheme is to be preferred, in which a cylindrical plasma shell (outer liner) is compressed by the magnetic field in the generator diode at a velocity of about $5 \cdot 10^5$ m/s and collides with an inner liner. Both liners are made of materials with a high atomic number. As a result of the generation of a strong shock wave in hypervelocity impacts, intense thermal x-ray emission takes place in the plasma of the inner liner, and this radiation penetrates into the liner cavity. At the same time, the outer liner confines the thermal energy, preventing the radiation from escaping outward, as a result of which the radiation intensity in the cavity is significantly increased. The condensed target that is to be irradiated can be positioned in the cavity of the liner or at one end.

In the work reported here, measurements were made of the intensities of the shock waves produced in condensed

aluminum and lead targets by intense pulses of soft x rays. In contrast to other studies,^{8–10} in which the radiation was generated by converting laser radiation into x rays, the present work used radiation lasting an order of magnitude longer (at the same power level) produced in the double liner scheme and resulting from the dynamic compression and heating of plasma with centripetal motion in the cylindrical Z-pinch geometry of the ANGARA-5 device.¹¹

2. THE DOUBLE-LINER MODEL AS SOURCE OF SOFT X RAYS. POWER PEAKING THROUGH LINER COLLISION

In contrast to the ideal double-liner scheme, in the experiments described here the outer liner was created by means of an annular nozzle, from which xenon is injected into the diode gap. The gas flow from the nozzle is not steady. For this reason, and also on account of viscous effects accompanying the gas flow into vacuum, the actual distribution of the gas density in the gap is quite broad and varies over the height of the gap. The effective value of the Mach number is $M = 4$.

To model the dynamics of the liners by means of a one-dimensional magnetohydrodynamic (MHD) code and estimate the effect of liner inhomogeneity along the axis on the radiation pulse, the liner was divided into three height zones. In each of the zones, the initial gas distribution of the outer liner was taken to be different and to correspond to experimental measurements and two-dimensional calculations of gas flow from a nozzle. The radiation outputs from the different zones were added together. The modeling was done by means of an MHD code based on the RAZRYaD software package,¹² augmented by the RD5 code of multigroup radiative transfer and by data on the equations of state, ionization kinetics, and the radiative properties of the materials. The number and arrangement of the groups were chosen with the aim of having, on the one hand, the minimum number of them in order to ensure the necessary rate of calculation of

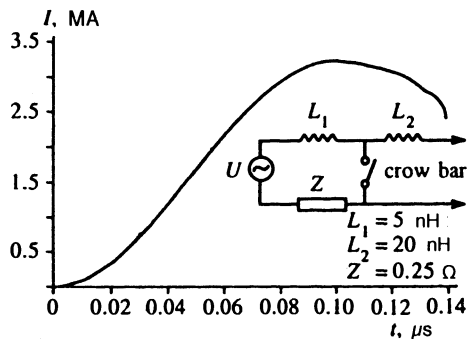


FIG. 1. Total current through the double liner device and equivalent circuit of the ANGARA-5 device.

the main physical processes and, on the other, the least error in the calculation of the radiation losses. Of course, the details of the spectrum are to a considerable degree lost in such a calculation. Indeed, strictly speaking, the accuracy with which it is possible at this stage to find the spectral absorption and emission coefficients for multielectron ions such as molybdenum and xenon cannot give us more than an order-of-magnitude estimate.

The mass of the outer xenon liner in the calculations was chosen to be $m_{Xe} = 160 \mu\text{g}$, and the mass of the inner molybdenum liner with agar-agar was $m_{Mo} = 250 \mu\text{g}$; its radius was 0.225 cm and thickness 0.025 cm. The height of both liners was 1 cm. The current through the double liner system was modeled by an electrical circuit equivalent to the output unit of the ANGARA-5 device. The circuit and a typical current pulse through the double liner system are shown in Fig. 1.

Figure 2 is a typical $R-t$ diagram: the dependences of the outer radius (R_1) of the xenon liner and of the outer (R_2) and inner (R_3) radii of the inner liner on the time.

The qualitative picture of the main physical processes that take place during the collapse and collision of the liners is as follows. As the magnetic-field pressure of the current through the liner increases in the gas (xenon in the given case), a current shell is formed, and a first shock wave is generated. Because of the strong radiative cooling of the multiply-charged plasma, the electron temperature is $T_e = 20-40 \text{ eV}$, and the thermal pressure is less than the magnetic pressure. The xenon plasma behind the shock wave is "swept up" into a shell with a thickness of about half the skin layer. After the shock wave has passed through the main mass of the gas shell, the liner is subsequently accelerated as

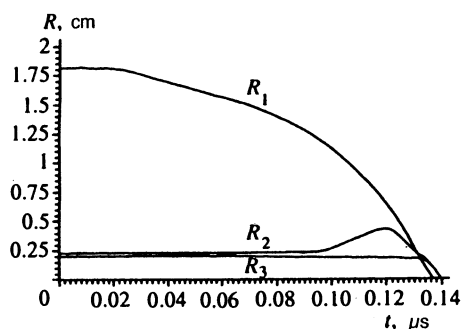


FIG. 2. The $R-t$ diagram of the doubler liner.

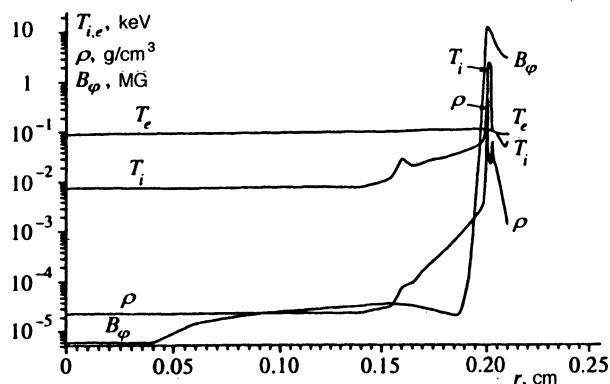


FIG. 3. Distribution of the plasma parameters: density ρ , magnetic field B_ϕ , ion temperature T_i , electron temperature T_e .

a whole. The shock wave continues to propagate through the decreasing density of the gas shell into the liner. Because of this, the shock wave is appreciably accelerated. As a result, the ion temperature T_i behind the shock wave increases strongly. The growth of T_i is also helped by the lowering in the rate of energy exchange with the electrons as a result of the low density. Here the plasma is strongly nonisothermal: $T_i \gg T_e$. The shock wave rapidly reaches the surface of the inner liner. Under the influence of the radiation of the outer liner and the hot ions of the low-density plasma, the outer layers of the inner liner sublime, forming a plasma corona.

The current in the system reaches a maximum of 3.3 MA at 95 ns after the beginning of the voltage pulse. After this, the crowbar regime of operation of the accelerator commences, in which the generator part is short-circuited by the plasma, and the current is maintained by virtue of the stored magnetic flux in the neighborhood of the liners and in the vacuum line. The magnetic field dissipates comparatively slowly because of the finite resistance of the plasma of the liners. At the time of the collision of the liners, the magnetic field, penetrating into the plasma, is compressed simultaneously with the density as the outer liner is compressed. The increasing magnetic field gives rise to a shock wave in the plasma of the inner liner and its corona. At the same time, the outer liner begins to be decelerated. At 129.5 ns, the kinetic energy of the liners reaches a maximum of 13.7 kJ. The distribution of the plasma parameters at this time is shown in Fig. 3.

Afterwards, the distribution of the magnetic field has a characteristic form with a maximum near the boundary between the outer moving liner and the inner liner at rest, ensuring deceleration of the former and generation of a shock wave in the latter. The outer liner is rapidly decelerated. The amplitude of the shock wave in the inner liner increases strongly, and since the liner plasma has a high $Z \gg 1$ the shock is accompanied by strong emission, mainly in bound-bound transitions.

In the given case, the shock wave, with a velocity of order $3 \cdot 10^7 \text{ cm/s}$, is supercritical. The material of the inner liner is chosen to ensure that the bulk of the thermal radiation penetrates the liner, filling, as it were, the cavity. The maximum intensity inside is reached at 131.2 ns. The electron temperature in the interior reaches 90 eV.

The radiation intensity in the cavity must be estimated with allowance for the fact that the shells do not collide simultaneously at all heights. Averaging of the radiation pulses from the different zones made with allowance for this yields an estimate for the maximum intensity of 4 TW/cm^2 for a pulse duration (at half-height) of 3 ns. An appreciable fraction of the kinetic energy of the outer liner is transformed into radiation. After the collision, both liners continue to be compressed by inertia, and they are somewhat accelerated by the effect of the magnetic pressure. Because of the large mass of the moving matter, its velocity does not exceed $2 \cdot 10^6 \text{ m/s}$. After $t_0 = 10 \text{ ns}$, the shells collapse onto the axis, and a Z-pinch is formed. The emission of the pinch reaches a maximum in the first compression and is characterized by the appearance of a second peak of soft x rays after the peak corresponding to the collision of the liners. The plasma then expands and contracts again. In the Z-pinch stage, the degree of compression reaches large values, and therefore various MHD instabilities necessarily begin to be manifested, so that the pinch dynamics becomes essentially three-dimensional and complicated. At this stage, the radiation power of the pinch can be estimated only on the basis of general energy considerations. Assuming that the current flows through some turbulent current shell, in general, we find that the specific power of the joule heating varies with the instantaneous value $I(t)$ of the current in accordance with the formula

$$W \cong \frac{I^2(t)}{\pi r^2 c^2 (t_0 + t)}, \quad (1)$$

where t is the time measured from the instant of the first compression, and r is the outer radius of the liner. Further, equating the radiation and the energy release, we can estimate the flux of radiation onto the target. It is obvious that the estimate will also depend on assumptions about the transparency of the plasma for the radiation. Limiting cases here could be either a surface or a bulk nature of the emission. In the immediate vicinity of the end of the liner (at a distance of 1–2 mm), the power of the radiation flux is in order of magnitude

$$P \approx \frac{I^2}{\pi r^2 c} \sqrt{\frac{1}{\sigma(t_0 + t)}}, \quad (2)$$

where σ is the conductivity of the current shell.

The spectral composition of the radiation is of particular interest. This is because the nonuniformity of the irradiation of the target depends on nonequilibrium processes in the pinch plasma, which determine the deviation of the radiation spectrum from equilibrium. Thus, the high-energy part has a decisive effect on the formation of a shock wave in the sample, this being due to the long range of the high-energy photons in matter.

The emission of the plasma at the time of collision is nonequilibrium on account of the finite optical thickness. The spectrum of the radiation in the cavity at temperature 90 eV as estimated in the multigroup approximation is shown in Fig. 4. The largest deviation from a Planck spectrum occurs at $\hbar\omega > 200 \text{ eV}$, where the plasma is almost transparent. Ra-

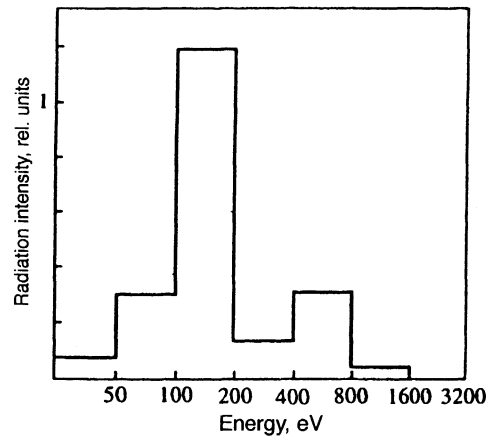


FIG. 4. Calculated pinch emission spectrum.

diation from the M shells of the molybdenum ions makes an appreciable contribution to the 400–800 eV group.

Deviation from the Planck spectrum can also be due to purely plasma effects. At high values of the electric field in the plasma, there can be an appreciable distortion of the electron distribution function due to the “runaway” effect, which occurs if $E > E_D(v_T/c)^2$ (Ref. 13), where

$$E_D = \frac{4\pi n_e e^3}{m_e v_T^2} \ln \Lambda. \quad (3)$$

The distribution function of electrons in a plasma that are in a static electric field E is appreciably modified at high velocities $v^2 > v_T^2 E_D/E$ and has the form¹⁴

$$f \approx \frac{m_e c}{(2\pi)^{3/2}} \frac{1}{v_T^3 p_l} \exp\left(-\frac{E_D}{4E} - \sqrt{\frac{2E_D}{E}} \frac{p_{tr}^2 c}{p_l T_{\text{eff}}}\right). \quad (4)$$

Here p_l and p_{tr} are the longitudinal and transverse momenta of the electrons, and

$$T_{\text{eff}} = \frac{E_D}{E} (1 + Z) T_e, \quad (5)$$

where T_{eff} is the “effective” temperature of the “runaway” electrons, which is appreciably higher than the temperature of the “bulk” of the electrons. The use of (4) gives the following result for the radiation spectrum in the intermediate range:

$$T_e \frac{E_D}{E} < \hbar\omega < T_{\text{eff}},$$

$$\frac{dI}{d\omega} = \frac{8}{3} \sqrt{\frac{2\pi Z^2 e^6 n_e n_i}{3 m_e^2 c v_T^3}} \frac{T_{\text{eff}}}{m_e c^2} \exp\left(-\frac{E_D}{4E} - \sqrt{\frac{2E_D}{E}} \ln\left(\frac{T_{\text{eff}}}{\hbar\omega}\right)\right). \quad (6)$$

An electric field of the order of hundreds of kilovolts per centimeter is applied to the diode gap. However, because of the motion of the liner the electric field in the plasma reaches values $\geq 50 \text{ kV/cm}$. Then the effective temperature for the parameters of the liner plasma is $T_{\text{eff}} \approx 10 \text{ keV}$, and this leads to an appreciable contribution of the runaway electrons to the

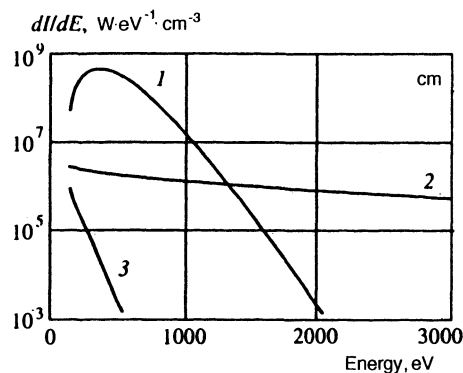


FIG. 5. Calculated spectra of electron bremsstrahlung: 1) Planck spectrum; 2) bremsstrahlung of the runaway electrons; 3) bremsstrahlung of the main bulk of the electrons.

high-energy region of the spectrum. Figure 5 gives calculated radiation spectra for the plasma parameters $T_e = 60$ eV and $n_e = 2 \cdot 10^{19} \text{ cm}^{-3}$, which are characteristic of the initial stage of the pinch. It can be seen that at energies greater than 1 keV the contribution of the fast electrons is decisive, and the spectral density of the radiation depends very weakly on the energy. This weak dependence is maintained up to an energy of order T_{eff} , and then decreases exponentially with increasing $\hbar\omega$.

3. NUMERICAL MODELING OF THE GENERATION OF SHOCK WAVES IN A CONDENSED TARGET UNDER THE INFLUENCE OF STRONG FLUXES OF SOFT X RAYS

The effect of strong fluxes of soft x rays on a condensed target leads to ablation of the target material and to the generation of a shock wave that propagates into the target. The equations that describe the motion of the matter with allowance for the transfer of thermal radiation are based on the conservation laws for the mass, momentum, and energy. Since in the considered problems the pressure and the energy density of the radiation are much less than the gas-dynamic pressure and the energy density of the matter, they can be ignored. This means that the momentum and energy equations have the same form as the equations of gas dynamics with a single difference—the flux of the radiation energy in the equation for the energy. Thus, the total energy changes as a result of the convective flux of the work of the pressure forces and the energy flux due to heat conduction and radiation. To determine the flux of the radiation energy (and also the density of the radiation energy, on which the flux depends), it is necessary to solve the equations of radiative transfer.

In the work reported here, the transfer of radiative energy was calculated in the multigroup diffusion approximation. The complete spectrum was divided into N groups. Within each group, the absorption coefficients were assumed to be independent of the frequency. The total flux of the radiation energy is the sum of the group fluxes, each of which is the solution of the system of equations of the diffusion approximation.

For the complete description of the process of interaction of the radiation with the matter, it is necessary to know both

the thermodynamic properties of the nonideal plasma realized in the region in which the energy is released and, accordingly, the coefficients of absorption in such a plasma as well as the equation of state for the strongly compressed matter in the region in which the shock wave propagates. In the present work, we used a ‘‘hybrid’’ equation of state, which is a linear superposition of models of ionization equilibrium¹⁵ for calculating the plasma thermodynamics and a wide-range equation of state¹⁶ constructed on the basis of shock-wave experiments and taking into account melting and evaporation. The switch from the one model to the other was made mainly on the basis of the degree of ionization of the matter calculated by means of the model of ionization equilibrium.

An important part in the solution of any problem of the interaction of radiation with a condensed barrier is the construction of the dependence of the mass absorption coefficient μ on the parameters of state of the medium: the density ρ , the temperature T , and the photon energy ε . These dependences are needed, first, to calculate the energy release resulting from the absorption of radiation from the external source in the barrier and the vapor formed from the material and, second, for the numerical modeling of the radiative energy transfer. Since in the process of interaction of matter with radiation the matter goes over from the dense condensed state to a rarefied, in some cases high-temperature, plasma, and the spectrum of its radiation lies in the soft x-ray and ultraviolet ranges, the dependence $\mu(\varepsilon, \rho, T)$ must be constructed using the following values of the variables: $\varepsilon = 10$ eV–1 keV, $\rho = 10^{-5}$ –100 g/cm³, and T up to 10^8 K. The problem of determining the coefficients over such wide parameter ranges is extremely complicated and has not been done for the majority of materials. An exception is one of the best studied metals—aluminum—but even there, only fragmentary data are given in the readily accessible sources.

Analysis of the various published sources on the coefficients of radiative absorption by aluminum made it possible to choose two of them as basis sources.^{17,18} Indeed, the data given in these studies agree satisfactorily with each other over the common parameter range and are fairly complete. The absorption coefficients in Ref. 17 were calculated with allowance for inverse bremsstrahlung, photoionization, and absorption in spectral lines. The photoionization cross sections were calculated in the dipole approximation and in Kramers’ classical approximation for highly excited levels. The absorption coefficients in lines were also calculated in the classical approximation with allowance for the natural, Stark, quadratic Stark, and Doppler mechanisms of line broadening. In addition, allowance was made for the cutoff of the upper excited levels of the ions in the plasma as a result of Coulomb interaction and the finite density.

The calculation of the absorption coefficients in Ref. 18 also took into account the inverse bremsstrahlung, photoionization, and line absorption. For temperatures above 100 eV, the Thomas–Fermi model was used, and at lower temperatures the Hartree–Fock–Slater model. These data have a number of shortcomings. The first is the coarse grid of photon energies, the considered interval of variation of which depends on T . In addition, it is not the ‘‘true’’ values of the

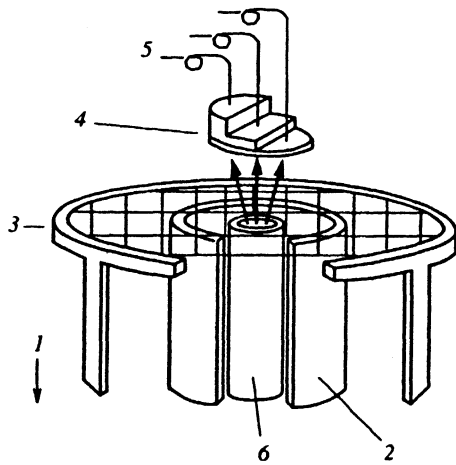


FIG. 6. Experimental layout: 1) cathode; 2) xenon gas jet; 3) anode; 4) target; 5) light guides; 6) inner liner.

absorption coefficients that are given in Ref. 18 but the coefficients obtained by Planck and Rosseland averaging over the energy intervals. However, as shown in Ref. 19, in problems of radiative gas dynamics it is necessary to use averaging over the true spectrum, which gives values of the absorption coefficients which, as a rule, lie between the Planck and Rosseland coefficients. Therefore, the data of Ref. 18 were used with appropriate interpolation.

In the program for calculating the coefficients using the data of Refs. 17 and 18, we used 22 energy points in the range from 10 to 1000 eV. These were chosen so as to take into account as fully as possible the details in the dependence of the absorption coefficients on the photon energy ε . To find μ at an arbitrary value of ε in a given range, logarithmic interpolation between neighboring energy grid points was used. The absorption coefficients at a point of the energy grid were calculated under the assumption that at temperatures below a certain T_0 the mass absorption coefficient does not change and is equal to μ_0 (values of μ_0 are given, for example, in the tables of Ref. 20). Using various physical arguments concerning the form of $\mu(E, \rho, T)$, we constructed interpolation and extrapolation formulas for each of the ranges of ρ and T . Thus, for the calculations we used either the data of Ref. 17 or the data of Ref. 18, or both. The equations of motion were integrated numerically by Godunov's method using a moving Lagrangian grid. To satisfy the specified accuracy in space, we used an algorithm for

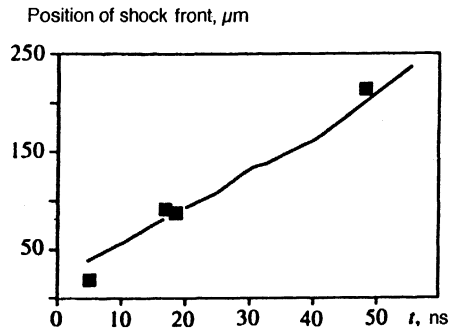


FIG. 7. Position of shock front for stepped target (aluminum 16 μm , lead up to 200 μm). The power level is 1.2 TW/cm^2 .

dividing the cells in the region of energy release as they became large with the expansion of the matter. The radiation energy fluxes and densities in the cells were calculated at each time step by solving the system of multigroup diffusion in accordance with the implicit scheme described in Ref. 21.

4. EXPERIMENTAL RESULTS OF MEASUREMENTS OF SHOCK WAVES GENERATED BY SOFT X-RAYS FROM THE Z PINCH IN THE ANGARA-5 DEVICE

To generate the radiating plasma, we used an inner liner in the form of a hollow cylinder consisting of a low-density agar-agar matrix implanted with molybdenum (cylinder density less than 10 mg/cm^3 , total mass up to 200 μg). The outer diameter of the liner was 4 mm, the wall thickness 0.2 mm, and the height of the liner 10 mm. The outer liner was a supersonic annular xenon jet of mass 150 μg , through which a pulsed current of magnitude 3.5 MA was passed.

The Z-pinch plasma emitted soft x rays with a nearly Planck spectrum and temperature of order 60–120 eV. This radiation was incident on a flat target positioned below the inner liner (distance 1 mm), consisting of layers of aluminum of thickness 16–32 μm and lead to thickness 80–200 μm . The experimental layout is shown in Fig. 6. The velocity of the shock wave was measured by means of optical baseline techniques²² using measurements of the time difference of arrival of the shock wave at the free surfaces of stepped targets. To extract the radiation from the experimental device, fiber optic transmission lines (quartz—polymer, length 80 m, loss 0.4 dB, transmission bandwidth 2 GHz) were used; they ensured good noise immunity of the detection apparatus.²³ The end of the fiber (diameter 400 μm) was

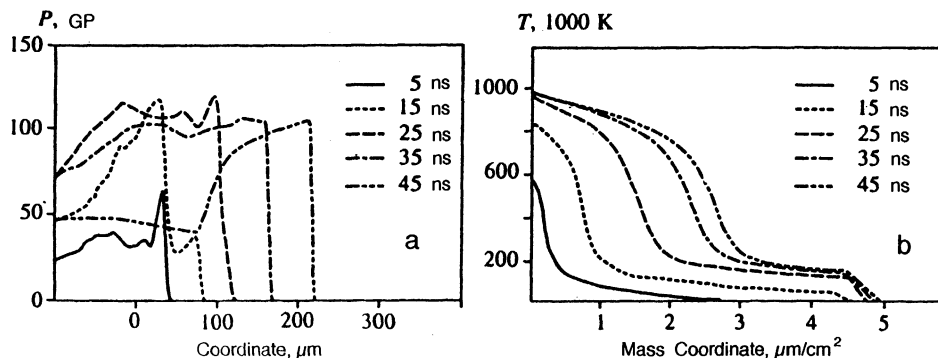


FIG. 8. Results of numerical modeling of the interaction of the soft x rays with the aluminum target: a) evolution of the pressure; b) evolution of the temperature. The peak power is 2 TW/cm^2 .

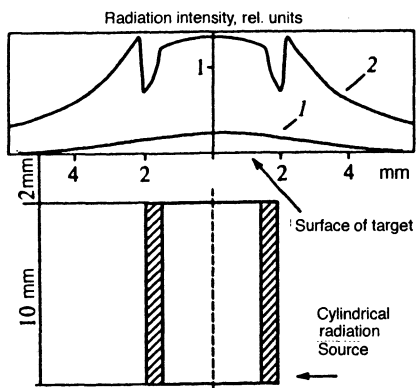


FIG. 9. Calculated distribution of the target irradiation intensity: 1) radiation from the bulk; 2) surface radiation.

directly next to the free surface of the sample; one fiber abutted the aluminum and the other the lead. The distance between the centers of the fibers at the target unit was 1 mm; for the diameter 4 mm of the irradiated target surface, this made it possible to ignore the spatial inhomogeneity of the radiation. To eliminate fiber emission under the influence of the hard x rays accompanying the generation of the pulse of soft x rays, the fibers were placed inside the working chamber in a steel tube, the end of which terminated at the experimental assembly. Optical emission from the fibers was detected by silicon photodiodes possessing a time resolution better than 1 ns. Analysis of the experimental results used the time difference between the leading edges of the signals (the time difference between the onset of emission), yielding time resolution better than 1.5 ns. The results of the experiments are presented in Fig. 7, which indicates the measured position of the shock front at different times. The mean propagation velocity of the shock wave on the 80- μm baseline was 7.3 ± 0.6 km/s, and on the 200- μm baseline it was 4.6 ± 0.3 km/s; on the basis of the shock adiabat of lead, these figures correspond to mean shock compression pressures of 3 Mbar and 0.9 Mbar, respectively.²⁴

The same figure gives the results of the numerical modeling. Figure 8 gives the calculated pressure and temperature profiles. In the calculations, we used the radiation spectra shown in Figs. 4 and 5; the radiation pulse width at half-height was taken to be 30 ns.

An important question in investigations of this kind is the degree of spatial homogeneity of the irradiated region. Under our conditions, the theoretical calculations predict an inhomogeneity of order 3%, which is due to the geometry of the experiment, as is demonstrated in Fig. 9, which gives the calculated spatial distribution of the radiation power at the target.

5. CONCLUSIONS

The results of the investigations showed that a Z-pinch plasma is a promising source for generating shock waves in

condensed targets. The greater duration of the radiation pulse compared with experiments in which shock waves are generated by the conversion of laser radiation into x rays makes it possible to increase the target thickness and, thus, significantly reduce the effect of sample preheating, which distorts the hydrodynamic picture of the process.

We are grateful to the team operating the ANGARA-5 device. This work was done with financial support by the Russian Fund for Fundamental Research (Projects Nos. 94-02-03430-a and 95-02-05141-a).

- ¹J. J. Duderstadt and G. P. Moses, *Inertial Confinement Fusion*, Wiley, New York (1984).
- ²S. I. Anisimov, A. M. Prokhorov, and V. E. Fortov, *Usp. Fiz. Nauk* **142**, 305 (1984) [*Sov. Phys. Usp.* **27**, 159 (1984)].
- ³D. L. Matthews, E. M. Campbell, N. M. Ceglo *et al.*, *J. Appl. Phys.* **54**, 4260 (1983).
- ⁴P. J. Turchi and W. L. Baker, *J. Appl. Phys.* **44**, 4936 (1973).
- ⁵S. V. Zakharov, L. B. Nikandrov, and V. P. Smimov, USSR Patent 1552889 [in Russian] November 22, 1989.
- ⁶V. P. Smimov, A. V. Branitskiĭ, E. I. Grabovskii *et al.*, in *Proceedings of the Eighth International Conference BEAMS-90* [in Russian], Novosibirsk (1990), p. 437.
- ⁷V. A. Gasilov, S. V. Zakharov, and V. P. Smimov, *Pis'ma Zh. Eksp. Teor. Fiz.* **53**, 83 (1991) [*JETP Lett.* **53**, 85 (1991)].
- ⁸T. Endo, H. Shiraga, K. Shihoyama *et al.*, *Phys. Rev. Lett.* **60**, 1022 (1988).
- ⁹Th. Lower and R. Sigel, in *Proceedings of the Seventh International Workshop on the Physics of Nonideal Plasmas*, Markgrafeneheide (1993).
- ¹⁰E. M. Campbell, *Laser and Part. Beams* **9**, 209 (1991).
- ¹¹E. P. Velikhov, V. P. Smimov, E. V. Grabovskii *et al.*, *At. Energ.* **68**, 26 (1990).
- ¹²V. A. Gasilov, S. V. Zakharov, A. Yu. Krukovskii, and K. V. Skorovarov, *Packs of Applied Programs. Ser. Algorithms and Algorithmic Languages* [in Russian], Nauka, Moscow (1991).
- ¹³A. V. Gurevich, *Zh. Eksp. Teor. Fiz.* **39**, 296 (1960) [*Sov. Phys. JETP* **12**, 209 (1961)].
- ¹⁴J. W. Connor and R. J. Hastie, *Nucl. Fusion* **15**, 415 (1975).
- ¹⁵W. Ebeling, A. Fuester, V. Fortov *et al.*, *Thermophysical Properties of Hot Dense Plasmas* (Teubner-Texte zur Physik, Vol. 25, Teubner-Verlag, Stuttgart (1991)).
- ¹⁶A. V. Bushman and V. E. Fortov, *Sov. Tech. Rev. B, Therm. Phys.* **1**, 219 (1987).
- ¹⁷V. P. Buzdin and I. B. Kosarev, Paper No. 534-75, All-Union Institute of Scientific and Technical Information [in Russian] (1975).
- ¹⁸*Absorption Coefficients of Light in Earth, Air, and Aluminum* [in Russian]. Report of the Institute of Applied Mineralogy, USSR Academy of Sciences (1984).
- ¹⁹I. V. Nemchinov, Paper No. 1721-83, All-Union Institute of Scientific and Technical Information [in Russian] (1983).
- ²⁰B. L. Henke, P. Lee *et al.*, *Atomic Data and Nuclear Data Tables* **27**, (1982).
- ²¹B. N. Chetverushkin, *Mathematical Modeling of Problems of the Gas Dynamics of Radiating Gases* [in Russian], Nauka, Moscow (1985).
- ²²L. V. Al'tshuler, A. A. Bakanova, A. V. Bushman *et al.*, *Zh. Eksp. Teor. Fiz.* **73**, 1866 (1977) [*Sov. Phys. JETP* **46**, 980 (1977)].
- ²³V. G. Ageev, A. V. Bushman, M. I. Kulish *et al.*, *JETP Lett.* **48**, 659 (1988).
- ²⁴A. V. Bushman, I. V. Lomonosov, and V. E. Fortov, *The Equation of State of Metals at High Energy Densities* [in Russian], Institute of Chemical Physics, Russian Academy of Sciences, Chernogolovka (1992).

Translated by Julian B. Barbour